Article

Characterization of Reactive Intermediates Generated During Photolysis of 4-Acetoxy-4-aryl-2,5-cyclohexadienones: Oxenium Ions and Aryloxy Radicals

Yue-Ting Wang, Kyoung Joo Jin, Samuel H. Leopold, Jin Wang, Huo-Lei Peng, Matthew S. Platz, Jiadan Xue, David Lee Phillips, Stephen A. Glover, and Michael Novak

J. Am. Chem. Soc., **2008**, 130 (47), 16021-16030 • Publication Date (Web): 31 October 2008

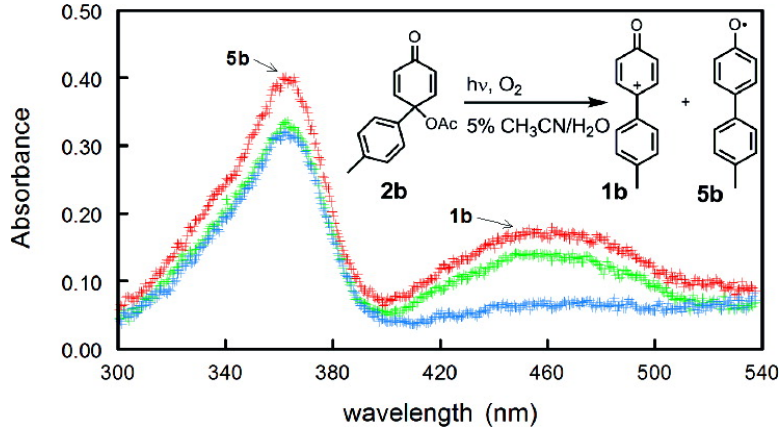

More About This Article

Additional resources and features associated with this article are available within the HTML version:

- Supporting Information
- Access to high resolution figures
- Links to articles and content related to this article
- Copyright permission to reproduce figures and/or text from this article

View the Full Text HTML

J|A|C|S
ARTICLES

Published on Web 10/31/2008

Characterization of Reactive Intermediates Generated During Photolysis of 4-Acetoxy-4-aryl-2,5-cyclohexadienones: Oxenium Ions and Aryloxy Radicals

Yue-Ting Wang,[†] Kyoung Joo Jin,[†] Samuel H. Leopold,[†] Jin Wang,[‡] Huo-Lei Peng,[‡] Matthew S. Platz,[‡] Jiadan Xue,[§] David Lee Phillips,[§] Stephen A. Glover,[||] and Michael Novak*,[†]

Department of Chemistry and Biochemistry, Miami University, Oxford, Ohio 45056, Department of Chemistry, The Ohio State University, 100 West 18th Avenue, Columbus, Ohio 43210, Department of Chemistry, University of Hong Kong, Hong Kong, P.R. China, and School of Biological, Biomedical, and Molecular Sciences, Division of Chemistry, University of New England, Armidale, 2351, New South Wales, Australia

Received July 10, 2008; E-mail: novakm@muohio.edu

Abstract: Aryloxenium ions **1** are reactive intermediates that are isoelectronic with the better known arylcarbenium and arylnitrenium ions. They are proposed to be involved in synthetically and industrially useful oxidation reactions of phenols. However, mechanistic studies of these intermediates are limited. Until recently, the lifetimes of these intermediates in solution and their reactivity patterns were unknown. Previously, the quinol esters **2** have been used to generate **1**, which were indirectly detected by azide ion trapping to generate azide adducts **4** at the expense of quinols **3**, during hydrolysis reactions in the dark. Laser flash photolysis (LFP) of **2b** in the presence of O_2 in aqueous solution leads to two reactive intermediates with λ_{max} 360 and 460 nm, respectively, while in pure CH_3CN only one species with λ_{max} 350 nm is produced. The intermediate with λ_{max} 460 nm was previously identified as **1b** based on direct observation of its decomposition kinetics in the presence of N_3^-, comparison to azide ion trapping results from the hydrolysis reactions, and photolysis reaction products (**3b**). The agreement between the calculated (B3LYP/6-31G(d)) and observed time-resolved resonance Raman (TR^3) spectra of **1b** further confirms its identity. The second intermediate with λ_{max} 360 nm (350 nm in CH_3CN) has been characterized as the radical **5b**, based on its photolytic generation in the less polar CH_3CN and on isolated photolysis reaction products (**6b** and **7b**). Only the radical intermediate **5b** is generated by photolysis in CH_3CN, so its UV−vis spectrum, reaction products, and decay kinetics can be investigated in this solvent without interference from **1b**. In addition, the radical **5a** was generated by LFP of **2a** and was identified by comparison to a published UV−vis spectrum of authentic **5a** obtained under similar conditions. The similarity of the UV−vis spectra of **5a** and **5b**, their reaction products, and the kinetics of their decay confirm the assigned structures. The lifetime of **1b** in aqueous solution at room temperature is 170 ns. This intermediate decays with first-order kinetics. The radical intermediate **5b** decomposes in a biphasic manner, with lifetimes of 12 and 75 μs. The decay processes of **5a** and **5b** were successfully modeled with a kinetic scheme that included reversible formation of a dimer. The scheme is similar to the kinetic models applied to describe the decay of other aryloxy radicals.

Introduction

Aryloxenium ions **1** are oxygen-centered cations in one of their canonical structures and are isoelectronic with well-known arylnitrenium and arylcarbenium ions. They have been proposed to be the reactive intermediates responsible for synthetically and industrially useful electrochemical and chemical oxidations of phenols.[1−5] For example, it has been proposed that they are responsible for the generation of commercially useful polymers, such as poly(2,6-dimethyl-1,4-phenylene oxide).[6,7] However, until recently mechanistic studies of **1** were fairly limited and

[†] Miami University.
[‡] The Ohio State University.
[§] University of Hong Kong.
[||] University of New England.

(1) (a) Swenton, J. S.; Carpenter, K.; Chen, Y.; Kerns, M. L.; Morrow, G. W. *J. Org. Chem.* **1993**, *58*, 3308–3316. (b) Swenton, J. S.; Callinan, A.; Chen, Y.; Rohde, J. L.; Kerns, M. L.; Morrow, G. L. *J. Org. Chem.* **1996**, *61*, 1267–1274.
(2) Rieker, A.; Beisswenger, R.; Regier, K. *Tetrahedron* **1991**, *47*, 645–654.
(3) Pelter, A.; Ward, R. S. *Tetrahedron* **2001**, *57*, 273–282.
(4) (a) Rieker, A.; Speiser, B.; Straub, H. *Dechema-Monographien* **1992**, *125*, 777–782. (b) Dimroth, K.; Umbach, W.; Thomas, H. *Chem. Ber* **1967**, *100*, 132–141.
(5) Rodrigues, J. A. R.; Abramovitch, R. A.; de Sousa, J. D. F.; Leiva, G. C. *J. Org. Chem.* **2004**, *69*, 2920–2928.
(6) (a) Baesjou, P. J.; Driessen, W. L.; Challa, G.; Reedjik, J. *J. Am. Chem. Soc.* **1997**, *119*, 12590–12594. (b) Driessen, W. L.; Baesjou, P. J.; Bol, J. E.; Kooijman, H.; Spek, A. L.; Reedjik, J. *Inorg. Chim. Acta* **2001**, *324*, 16–20.
(7) Kobayashi, S.; Higashimura, H. *Prog. Polym. Sci.* **2003**, *28*, 1015–1048.

little was known about the generation, reactivity, and selectivity of these species, or even whether they have actually been produced in the reactions in which they have been invoked.[1,3,5] Prior to our investigations only a few highly delocalized examples of **1**, such as **1d** and **1e**, were observed or isolated.[4] More recently, the very long-lived oxenium ion derived from α-tocopherol has been investigated.[8] Unfortunately, these unusually stabilized species provided little understanding of the reactions of this class of transient ions. Furthermore, the previously existing mechanistic studies of these species were not consistent with each other.[9−13] Discrepancies existed concerning the regiochemistry of reactions of purported **1** generated from different sources and the possible involvement of triplet ions.[2,9,11,13] In most cases unequivocal evidence for the existence of the cations was not presented.[2,9−12]

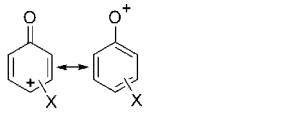

1 **a** X = 4-Ph
b X = 4-(4′-MeC_6H_4)
c X = 4-(4′-BrC_6H_4)
d X = 2,4,6-(4′-$MeOC_6H_4$)
e X = 2,6-*t*-Bu-4-(4′-$(Me_2N)C_6H_4$)

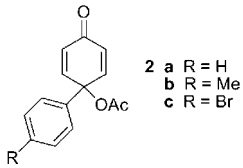

2 **a** R = H
b R = Me
c R = Br

Several years ago we initiated a study of the chemistry of aryloxenium ions. We were able to indirectly detect the generation of 4′-substituted-4-biphenylyloxenium ions **1a−c** from catalyzed or uncatalyzed solvolysis of **2a−c** through N_3^--trapping, common ion effects, and ^{18}O-labeling studies in $^{18}O-H_2O$.[14−16] More recently, we succeeded in directly observing the generation and decomposition of **1b** by laser flash photolysis (LFP) in aqueous solution.[17] This transient ion with λ_{max} 460 nm was characterized initially by the kinetics of its reaction with N_3^-. The second-order reaction of **1b** with N_3^- is apparently diffusion limited, and the rate constant ratio k_{az}/k_s

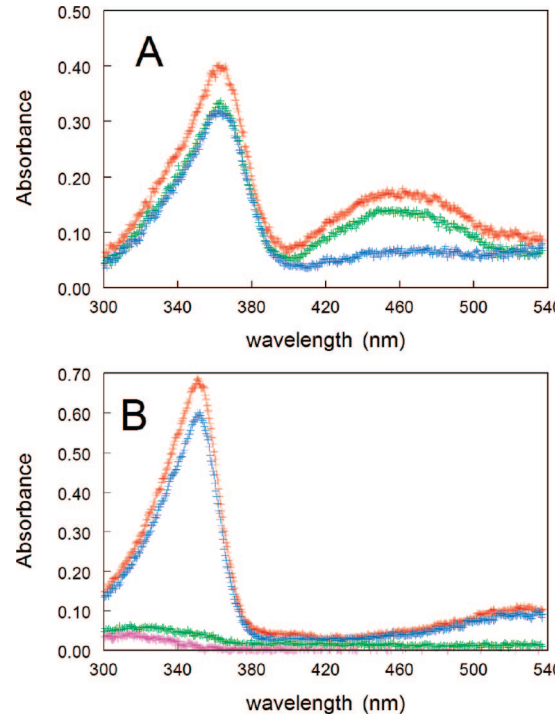

Figure 1. Transient absorbance spectra obtained after 266 nm excitation of **2b** in O_2-saturated pH 7.1 phosphate buffer (A) or in O_2-saturated CH_3CN (B). Key for A: red, 20 ns after flash; green, 120 ns; blue, 220 ns. Key for B: red, 20 ns after flash; blue, 1 μs; green, 100 μs; magenta, 200 μs. All spectra recorded over a 20 ns window.

Scheme 1. Photolysis of **2a** and **2b**

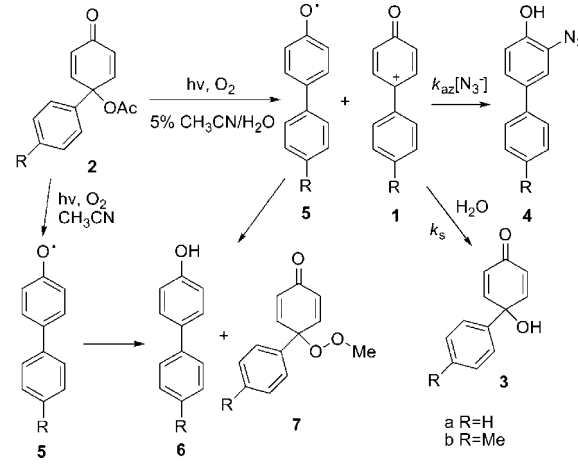

(Scheme 1) measured directly from the kinetics of decomposition of **1b** is equivalent, within experimental error, to the same ratio calculated from the yields of **4b** and **3b** during the hydrolysis of **2b** in N_3^--containing aqueous buffers. A second longer-lived transient intermediate with λ_{max} 360 nm was not identified.[17]

In this paper, further characterization of **1b** and the identification of the other observed reactive species are presented. For **1b**, a nanosecond time-resolved resonance Raman (ns-TR^3) spectrum has been recorded and compared with vibrational transitions calculated by DFT methods (B3LYP/6-31G(d)). These results confirm our assignment of the 460 nm absorbance band to **1b** and strongly indicate that the properties of **1b** are predominately those expected for its 1-oxo-2,5-cyclohexadienyl carbenium ion resonance structure as previously indicated by

(8) (a) Williams, L. L.; Webster, R. D. *J. Am. Chem. Soc.* **2004**, *126*, 12441–12450. (b) Lee, S. B.; Lin, C. Y.; Gill, P. M.; Webster, R. D. *J. Org. Chem.* **2005**, *70*, 10466–10473.
(9) (a) Abramovitch, R. A.; Inbasekaran, M.; Kato, S. *J. Am. Chem. Soc.* **1973**, *95*, 5428–5430. (b) Abramovitch, R. A.; Alvernhe, G.; Inbasekaran, M. N. *Tetrahedron Lett.* **1977**, 1113–1116. (c) Abramovitch, R. A.; Inbasekaran, M. N. *J. Chem. Soc., Chem. Commun* **1978**, 149–150. (d) Abramovitch, R. A.; Alvernhe, G.; Bartnik, R.; Dassanayake, N. L.; Inbasekaran, M. N.; Kato, S. *J. Am. Chem. Soc.* **1981**, *103*, 4558–4565.
(10) Li, Y.; Abramovitch, R. A.; Houk, K. N. *J. Org. Chem.* **1989**, *54*, 2911–2914.
(11) (a) Endo, Y.; Shudo, K.; Okamoto, T. *J. Am. Chem. Soc.* **1977**, *99*, 7721–7723. (b) Shudo, K.; Orihara, Y.; Ohta, T.; Okamoto, T. *J. Am. Chem. Soc.* **1981**, *103*, 943–944. (c) Endo, Y.; Shudo, K.; Okamoto, T. *J. Am. Chem. Soc.* **1982**, *104*, 6393–6397.
(12) Uto, K.; Miyazawa, E.; Ito, K.; Sakamoto, T.; Kikugawa, Y. *Heterocycles* **1998**, *48*, 2593–2600.
(13) Hegarty, A. F.; Keogh, J. P. *J. Chem. Soc., Perkin Trans. 2* **2001**, 758–762.
(14) Novak, M.; Glover, S. A. *J. Am. Chem. Soc.* **2004**, *126*, 7748–7749.
(15) Novak, M.; Glover, S. A. *J. Am. Chem. Soc.* **2005**, *126*, 8090–8097.
(16) Novak, M.; Poturalski, M. J.; Johnson, W. L.; Jones, M. P.; Wang, Y.; Glover, S. A. *J. Org. Chem.* **2006**, *71*, 3778–3785.
(17) Wang, Y.-T.; Wang, J.; Platz, M. S.; Novak, M. *J. Am. Chem. Soc.* **2007**, *129*, 14566–14567.

Table 1. Rate Constants Obtained from LFP Experiments[a]

intermediate	reaction conditions	rate constant (units), wavelength monitored	value
1b	5 vol% CH_3CN/H_2O, O_2 sat	k_{az} (M^{-1} s^{-1}), 460 nm	$(6.6 \pm 0.2) \times 10^{9b}$
1b	5 vol% CH_3CN/H_2O, O_2 sat	k_s (s^{-1}), 460 nm	$(5.8 \pm 0.4) \times 10^{6b}$
5b	5 vol% CH_3CN/H_2O, O_2 sat	k_{1AQ}^{O2} (s^{-1}), 360 nm	$(8.06 \pm 0.08) \times 10^4$
5b	5 vol% CH_3CN/H_2O, O_2 sat	k_{2AQ}^{O2} (s^{-1}), 360 nm	$(1.29 \pm 0.02) \times 10^4$
5b	CH_3CN, O_2 sat	k_{1ACN}^{O2} (s^{-1}), 350 nm	$(11.0 \pm 0.7) \times 10^4$
5b	CH_3CN, O_2 sat	k_{2ACN}^{O2} (s^{-1}), 350 nm	$(2.35 \pm 0.07) \times 10^4$
5b	CH_3CN, O_2 sat	k_{1ACN}^{O2} (s^{-1}), 575 nm	$(13.2 \pm 0.6) \times 10^4$
5b	CH_3CN, O_2 sat	k_{2ACN}^{O2} (s^{-1}), 575 nm	$(2.82 \pm 0.32) \times 10^4$
5b	CH_3CN, Ar sat	k_{1ACN}^{Ar} (s^{-1}), 350 nm	$(7.18 \pm 0.57) \times 10^4$
5b	CH_3CN, Ar sat	k_{2ACN}^{Ar} (s^{-1}), 350 nm	$(1.18 \pm 0.09) \times 10^4$
5b	CH_3CN, Ar sat	k_{1ACN}^{Ar} (s^{-1}), 575 nm	$(7.83 \pm 0.30) \times 10^4$
5b	CH_3CN, Ar sat	k_{2ACN}^{Ar} (s^{-1}), 575 nm	$(1.19 \pm 0.11) \times 10^4$
5a	CH_3CN, O_2 sat	k_{1ACN}^{O2} (s^{-1}), 340 nm	$(5.56 \pm 0.48) \times 10^4$
5a	CH_3CN, O_2 sat	k_{2ACN}^{O2} (s^{-1}), 340 nm	$(6.85 \pm 1.70) \times 10^3$

[a] All rate constants were collected at 22 °C under the conditions described in the Table. Rate constants and error limits for **5a** and **5b** are averages and standard deviations of three to five independent measurements. Rate constants for **1b** were determined as described in ref 17. [b] Determined from the slope (k_{az}) or intercept (k_s) of a plot of k_{obs} vs [N_3^-] at six [N_3^-] at 0−4 mM (see ref 17).

the experimental properties and calculated structures of **1b** and related ions.[14−18] The other long-lived intermediate generated along with **1b** under the same conditions has been identified as radical **5b**. This is the only reactive intermediate generated by LFP of **2b** in CH_3CN. We have also detected the generation of **5a** during LFP of **2a** in both pH 7.1 aqueous buffer and CH_3CN. The identity of **5a** can be confirmed by comparison of its UV−vis spectrum to that of authentic **5a**.[19,20] Photolysis reaction products (**6** and **7**) derived from both intermediates **5a** and **5b** have been isolated and characterized for both quinol esters **2a** and **2b**. The kinetics of the decomposition of **5a** and **5b** have been successfully modeled by a kinetic scheme that includes reversible formation of a dimer. The scheme is similar to the kinetic models applied to describe the decay of other aryloxy radicals.[21−28]

Results and Discussion

Laser flash photolysis of **2b** (2.5×10^{-4} M) at 266 nm in O_2-saturated pH 7.1, 0.02 M phosphate buffer (5 vol% CH_3CN/H_2O, $\mu = 0.5$ ($NaClO_4$), 22 °C) generates two transient absorption bands that can be detected within 20 ns after the flash. These bands with λ_{max} 460 and 360 nm, respectively, decay at significantly different rates (Figure 1A) and therefore must be associated with two different species. The intermediate with λ_{max} 460 nm decays in a first-order manner with a lifetime of (170 ± 10) ns. This species was identified as the oxenium ion **1b** because it reacts rapidly with N_3^- with an apparently diffusion-limited second-order rate constant, k_{az}, of (6.6 ± 0.2) × 10^9 M^{-1} s^{-1} (Table 1), and its lifetime is insensitive to the presence of O_2.[17] Further confirmation of the structural assignment was obtained from the equivalence of the k_{az}/k_s ratio measured from LFP of **2b** ((1.14 ± 0.09) × 10^3 M^{-1}) with the same ratio measured from the N_3^--trapping product study of **2b** in identical aqueous solutions at 30 °C of (1.0 ± 0.2) × 10^3 M^{-1}.[16] Steady state photolysis confirmed that a major photolysis product of **2b** is the quinol **3b**.[17] This is the expected product of the reaction of **1b** with the aqueous solvent and is the only detected product of the hydrolysis of **2b**.[16]

Time-Resolved Resonance Raman Characterization of the Oxenium Ion. Nanosecond time-resolved resonance Raman (ns-TR^3) spectra were obtained at room temperature in phosphate buffered 20 vol% CH_3CN/H_2O and in CH_3CN on freshly prepared 2 mM solutions of **2b**. A pump laser pulse of 266 nm, identical to that used for the LFP studies, was used to generate transient species. Laser pulses of 354.7 and 435.7 nm were used to probe the transients. These two probe pulses are within the absorption bands for the 360 and 460 nm species observed by LFP. TR^3 spectra were recorded on freshly prepared buffered aqueous solutions of **2b**, but no signal was observed 10 min after mixing **2b** with buffered water. This is consistent with the known rapid decomposition of **2b** in water.[16] Figure 2 shows the 435.7 nm TR^3 spectra obtained in 20 vol% CH_3CN/H_2O (A) and in CH_3CN (B) 10 ns after flash photolysis of **2b**. The scaled difference spectrum (diff = (A − B)) was generated to remove the band υ_{11} contribution of (B) from (A). The vibrational frequencies obtained from the difference spectrum are tabulated in Table 2 with the calculated frequencies obtained from the fully optimized structure of **1b** at the B3LYP/6-31G(d) level of theory. The tabulated frequencies for spectra (A) and (B) are available in the Supporting Information (Table S1).

The assigned vibrational modes in the 1100−1700 cm^{-1} range include all of the most intense predicted IR (IR1−IR4) and Raman (R1−R7) active modes from the frequency calculations (the vibrational modes are shown in Figure S1 in the Supporting Information). Agreement between the calculated and observed frequencies is generally good (< ±25 cm^{-1} for 8 of 11 assigned bands), but some modes, notably R1 and IR3, have discrepancies between calculated and observed frequencies of ca. 35 cm^{-1}. Figure 3 shows a simulation of the observed Raman spectrum obtained by scaling the calculated IR and Raman intensities independently of each other to match the intensities of the observed spectrum.

(18) Glover, S. A.; Novak, M. *Can. J. Chem.* **2005**, *83*, 1372–1381.
(19) Das, T. M.; Neta, P. *J. Phys. Chem. A* **1998**, *102*, 7081–7085.
(20) Das, P. K.; Encinas, M. V.; Steenken, S.; Scaiano, J. C. *J. Am. Chem. Soc.* **1981**, *103*, 4162–4166.
(21) Land, E. J.; Porter, G. *Trans. Faraday Soc.* **1963**, *59*, 2016–2026.
(22) Dobson, G.; Grossweiner, L. I. *Trans. Faraday. Soc.* **1965**, *61*, 708–714.
(23) Weiner, S. A. *J. Am. Chem. Soc.* **1972**, *94*, 581–584.
(24) Mahoney, L. R.; Weiner, S. A. *J. Am. Chem. Soc.* **1972**, *94*, 585–590.
(25) Weiner, S. A.; Mahoney, L. R. *J. Am. Chem. Soc.* **1972**, *94*, 5029–5033.
(26) Parnell, R. D.; Russell, K. E. *J. Chem. Soc., Perkin Trans. 2* **1974**, 161–164.
(27) Kuzmin, V. A.; Khudjakov, I. V.; Levin, P. P., Jr.; Emanuel, N. M.; De Jonge, C. R. H. I.; Hageman, H. J.; Biemond, M. E. F.; van der Maeden, F. P. B.; Mijs, W. J. *J. Chem. Soc., Perkin Trans. 2* **1979**, 1540–15444.
(28) Becker, H.-D. *J. Org. Chem.* **1965**, *30*, 982–989.

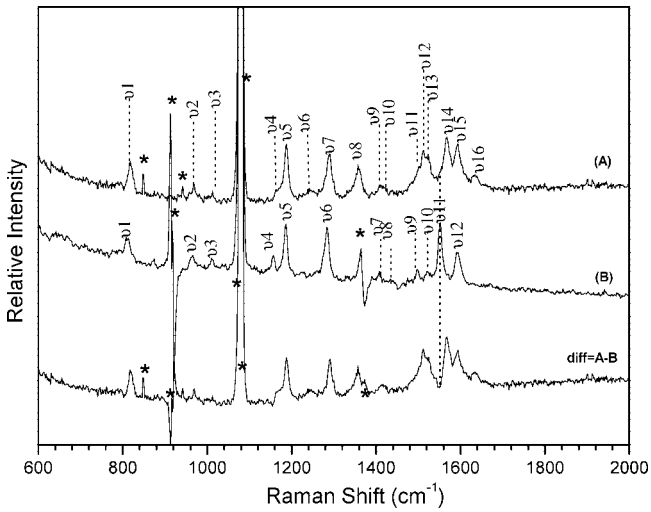

Figure 2. 435.7 nm resonance Raman spectra obtained 10 ns after 266 nm photolysis of **2b** in mixed aqueous solution (A) and pure CH_3CN (B). The bottom curve (diff = A − B) is obtained by subtracting the scaled (B) from (A), removing the band ν11 contribution of (B) from (A). Star symbols mark solvent-subtraction artifacts, stray-light, and ambient-light artifacts.

Table 2. Comparison of the Experimental and Calculated Vibrational Frequencies for **1b**

	vibrational mode description	B3LYP/6-31G(d) calcd value (cm^{-1})	transient resonance Raman frequency shift (cm^{-1})
			817
			969
R7	ArCH bend	**1167**	**1164**
IR4	Ar′CH bend, C—CH_3 stretch	**1184**	**1188**
		1212	
R6	Ar′CH bend, C—CH_3 stretch	**1226**	**1241**
		1272	
		1308	
IR3	Ar—Ar′ stretch	**1328**	**1290**
		1340	
R5	CH_3 bend	**1373**	**1357**
		1391	
IR2	ArCH bend, Ar—Ar′stretch	**1411**	**1418**
		1426	
		1438	
		1452	
R4	Ar′ angle deformation	**1495**	**1512**
		1500	
R3	ArC═C asym. stretch	**1542**	**1525**
IR1	Ar′C═C sym. stretch	**1596**	**1568**
R2	ArC═C sym stretch	**1616**	**1593**
R1	CO stretch	**1672**	1635

TR^3 spectra taken in mixed aqueous solvent and in CH_3CN with the 354.7 nm probe pulse are different from those taken with the 435.7 nm probe (Figures S2 and S3 in the Supporting Information). The spectrum recorded in the aqueous solvent resembles spectrum (A) in Figure 2, but the relative peak intensities are different and the Raman shifts are somewhat different. Since we know that the absorbance at 360 nm observed in the LFP experiments is predominately not due to **1b**, and **1b** is not generated by LFP in CH_3CN (below), these results are not surprising. There does appear to be some absorbance due to **1b** at 360 nm, so it is possible that the aqueous solution TR^3 spectrum taken with the 354.7 nm probe contains some contributions from **1b**.

The optimized geometry of **1b** is depicted in Figure 4 (the optimized Z-matrix is given in Table S2 in the Supporting Information). There is a small inter-ring dihedral angle of 14°

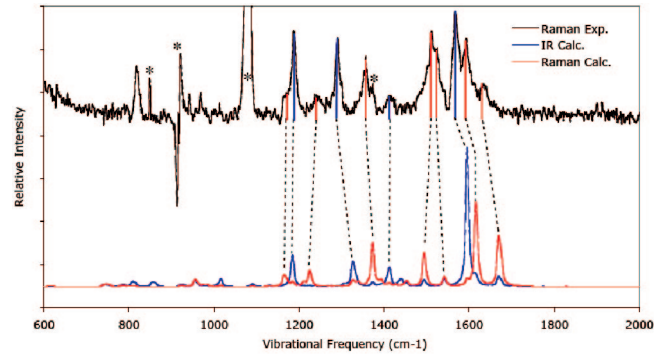

Figure 3. Observed and simulated vibrational spectrum of **1b**. The simulated spectrum was obtained by independently scaling the calculated intensities of the IR active bands (blue) and the Raman active bands (red).

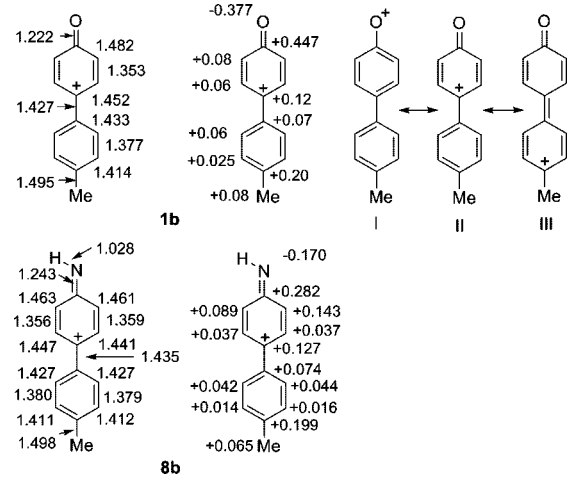

Figure 4. Calculated (B3LYP/6-31G(d)) bond lengths (Å), Mulliken charges (charges on H summed into heavy atoms), and dominant resonance structures for **1b** and the corresponding nitrenium ion, **8b**.

at this level of theory. At the HF/6-31G* level of theory the cation is planar. There is good evidence for strong bond alternation throughout the biphenyl moiety, and the C—O bond length of 1.222 Å is typical of a carbonyl. This suggests the oxenium ion has significant cyclohexadienyl character in the phenyl rings and carbonyl character in the carbon—oxygen bond. This is similar to the significant cyclohexadienyl character in the phenyl rings and imine character in the carbon—nitrogen bond of the analogous 4-biphenylylnitrenium ion previously studied by TR^3 spectroscopy and DFT calculations.[29] The highest frequency Raman band in the gas phase, corresponding to a C—O stretch, is also typical of a carbonyl (1672 cm^{-1} after scaling). The observed Raman shift is somewhat lower at 1635 cm^{-1}, but still within the range of a carbonyl with significant π-delocalization. We note that hydrogen bonding of water at the carbonyl bond has been previously observed to noticeably downshift the C═O stretching Raman band for aromatic carbonyls like *para*-methoxyacetophenone from ~1695 cm^{-1} in cyclohexane to ~1672 cm^{-1} in a 50% H_2O/50% CH_3CN (v/v) solvent.[30] This is quite similar to the downshift in the vibrational frequency observed for the analogous C═O Raman

(29) Zhu, P.; Ong, S. Y.; Chan, P. Y.; Poon, Y. F.; Leung, K. H.; Phillips, D. L. *Chem.—Eur. J.* **2001**, *7*, 4928–4936.
(30) Chan, W. S.; Ma, C.; Kwok, W. M.; Phillips, D. L. *J. Phys. Chem. A* **2005**, *109*, 3454–3469.

band in the spectrum of the oxenium ion (from 1672 cm^{-1} for the DFT gas phase calculation to the experimental 1635 cm^{-1} seen in the aqueous solution where hydrogen bonding of the carbonyl is very likely significant). Thus, the hydrogen bonding of water to the C−O bond most likely accounts for the larger difference in the Raman vibrational frequencies observed between the gas phase DFT predicted frequency for the C═O stretch Raman band and that actually observed in the experimental TR^3 spectrum for the oxenium ion. Mulliken atomic charges confirm delocalization of the positive charge into the 4-*para*-tolyl substituent. Group charges on the substituent ring account for 0.52 of the total charge, and charge is concentrated upon both C-4 (+0.12) and C-4′ (+0.2). The carbonyl bears a charge of only +0.07. The dipole moment of 4.45 D is directed along the longitudinal axis of the molecule, as expected. In valence bond terms, resonance structures II and III, rather than I (Figure 4), are dominant. We have found similar results for **1a** from calculations at the HF/6-31G* and pBP/DN*//HF/6-31G* levels of theory.[18] The agreement between the calculated and observed vibrational spectrum for **1b** indicates that the calculated properties of the cation do reproduce those of the actual cation.

The computed properties of the analogous nitrenium ion **8b** (Table S3 in the Supporting Information) at the B3LYP/6-31G(d) level are similar to **1b**. Less charge is localized into the 4-*para*-tolyl substituent (+0.45) though Mulliken charges at the C-4 and C-4′ positions are similar. There is a slightly larger inter-ring dihedral angle of 16.7°. This and the longer inter-ring bond indicate less resonance through to the 4-*para*-tolyl substituent. Bond alternation is also somewhat reduced throughout the structure, and nearly twice as much positive charge resides on the CNH of **8b** (0.112) than on the CO of **1b**. The dipole moment of 1.479 D is considerably modified by the NH bond. The component of the dipole moment along the C−N bond, corrected for the N−H bond contribution, is estimated to be 1.22 D, considerably less than the dipole moment of **1b**. Similar differences in calculated properties have been noted for other aryloxenium ions, including **1a**, and their analogous arylnitrenium ions at the HF/6-31G* and BP/DN*//HF/6-31G* levels of theory.[18]

It is initially surprising that the IR active bands (IR1−4) appear as significant bands in the TR^3 spectrum of **1b**. Figure 4 shows that the strong IR bands are also weakly allowed in the calculated Raman spectrum due to the low symmetry of **1b**. However, the observed intensities of the TR^3 spectrum are quite different from the calculated Raman intensities. The intensities of resonance Raman spectra can be very different from those observed or calculated in Raman spectra obtained under nonresonant conditions.[31] The probe Raman excitation wavelength is in resonance with an electronic transition of the species being probed. The bands in the resonance Raman spectrum associated with vibrational modes of molecular components that undergo a significant change in structure in the excited state relative to the ground state will be enhanced.[31] For example, selective probe wavelength-dependent resonance Raman enhancement of bands assigned to vibrational modes of the benzoin chromophore in benzoin diethyl phosphate has been demonstrated.[31a] In the present example, the Raman bands R1 and R2 and the IR band IR1 are C═O, ArC═C, and Ar′C═C stretch modes and are fairly intense bands in the TR^3 spectrum.

(31) (a) Chan, W. S.; Ma, C.; Kwok, W. M.; Zuo, P.; Phillips, D. L. *J. Phys, Chem. A* **2004**, *108*, 4047–4058. (b) Du, Y.; Ma, C.; Kwok, W. M.; Xue, J.; Phillips, D. L. *J. Org. Chem.* **2007**, *72*, 7148–7156.

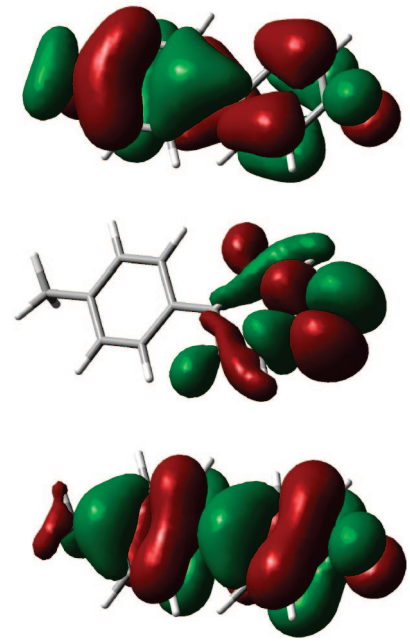

Figure 5. $HOMO^{-1}$ (π, top), nonbonding (π_Y, middle), and LUMO (π, bottom) orbitals for **1b** calculated at the B3LYP/6-31G(d) level.

The $HOMO^{-1}$ (π), nonbonding (π_Y), and LUMO (π) orbitals are depicted in Figure 5. The $\pi-\pi^*$ and $n-\pi^*$ transitions lead to changes in bond order of the ArC═C and Ar′C═C as well as the C═O bonds and hence the lengths of these bonds in the excited state. This change in excited-state structure would be expected, as observed, to enhance vibrational modes associated with changes in these bond lengths.

Characterization of the Aryloxy Radical. The decay of the transient absorbance at 360 nm in Figure 1A occurs in a biphasic manner. The absorbance vs time data at $t \geq 1$ μs (to avoid complications from absorbance of **1b** at that wavelength) can be fit to an equation containing two first-order rate constants (k_{1AQ}^{O2} and k_{2AQ}^{O2}) that are not dependent on [N_3^-]. All rate constants are reported in Table 1.The lifetimes of these decay processes (12 and 75 μs) are significantly longer than that of **1b**.[17] Assignment of the 360 nm absorbance band to a radical intermediate **5b** was based on the LFP generation of the same intermediate in CH_3CN, comparison of the observed UV−vis spectra attributed to **5a** and **5b** with previously published spectra for **5a**,[19,20] isolated photolysis reaction products of **2a** and **2b** that are attributable to **5a** and **5b**, and modeling of the decay kinetics of **5a** and **5b**.

LFP of **2b** in O_2-saturated CH_3CN (Figure 1B) apparently generates only one transient. The absorbance observed at 460 nm in aqueous solution that was assigned to **1b** has disappeared. The strong transient absorbance band at shorter wavelengths remains, but λ_{max} has shifted to ca. 350 nm. A much weaker band at longer wavelengths (>460 nm) is also observed. Both of these bands disappear with biphasic first-order kinetics and with equivalent rate constants (Table 1). This indicates that both absorbance bands are associated with the same intermediate. The magnitudes of these rate constants (k_{1ACN}^{O2} and k_{2ACN}^{O2}) are similar to those observed for the decay of the 360 nm band in O_2-saturated aqueous solution indicating that this absorbance band is due to a neutral intermediate not strongly affected by solvation that is equivalent to the intermediate with λ_{max} 360 nm detected in water. The lack of generation of **1b** in the CH_3CN solutions is consistent with solvation-based destabiliza-

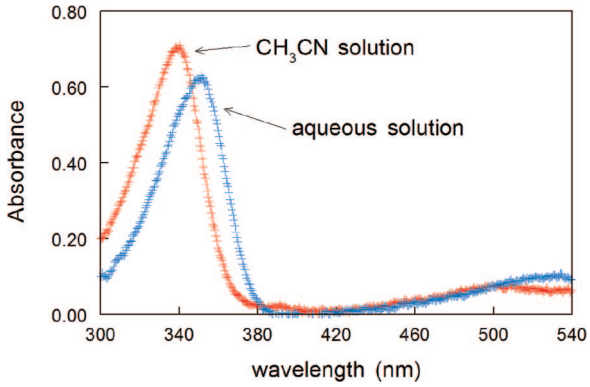

Figure 6. Transient absorbance spectra obtained 20 ns after 266 nm excitation of **2a** in O_2-saturated pH 7.1 phosphate buffer (blue) or in O_2-saturated CH_3CN (red). Spectra recorded over a 20 ns window.

tion of the transition state leading to the cation in CH_3CN under conditions in which a competing homolytic photolysis to generate **5b** is not strongly affected by the solvent. In Ar-saturated CH_3CN the band at 350 nm and the weak long wavelength band are still observed. In addition, a prominent shoulder at 400 nm that disappears within 10 μs is detected (Figure S4 in the Supporting Information). This rapidly decaying transient absorbance does not interfere with the decay of the two major absorbance bands. Monitoring of the kinetics at 350 and 575 nm shows that the intermediate disappears in a biphasic manner with rate constants (k_{1ACN}^{Ar} and k_{2ACN}^{Ar}). The magnitudes of these rate constants are somewhat smaller than those observed in the presence of O_2.

Results of LFP of **2a** in O_2-saturated pH 7.1 phosphate buffer or in O_2-saturated CH_3CN are shown in Figure 6. No transient that can be assigned to **1a** is detected in the aqueous solution. Although steady state photolysis product studies indicate that some **1a** is formed (below), it is not surprising that it was not detected in the ns-LFP experiments because the lifetime of **1a** estimated from an N_3^--trapping product study performed during hydrolysis of **2a** under the same aqueous conditions is only 12 ns.[14] Monitoring absorbance vs time at 450 nm (near λ_{max} for **1b**) at early reaction times reveals an apparent fluorescence that decays within 15 ns after the flash. After that, slow decay of the signal occurs on a longer 10−100 μs time scale. The fluorescence signal would obscure any absorbance due to **1a** at short reaction times within the estimated lifetime of **1a**. The LFP results confirm our previous conclusions based on N_3^--trapping of hydrolysis reactions of oxenium ion precursors that the aqueous solution lifetimes of 4′-substituted-4-biphenylyloxenium ions are highly dependent on the nature of the 4′-substituent.[16] These results are also in agreement with the calculations that show significant delocalization of the positive charge into the distal rings of these cations.[16−18]

Although **1a** was not detected, another transient with λ_{max} 350 nm was detected in aqueous solution. In CH_3CN a transient is generated with λ_{max} 340 nm. This solvent shift is equivalent to that observed for **5b**, although in both solvents the transient absorption maximum for **5b** is shifted to a longer wavelength by ca. 10 nm. In both solvents a weaker absorbance band, apparently associated with the same transient, is observed at $\lambda > 460$ nm. The spectrum observed in aqueous solution is indistinguishable from that previously observed during pulse radiolysis of N_2O-saturated aqueous solutions of **6a** that was attributed to **5a**.[19] A very similar absorbance spectrum attributed to **5a** was observed in 1:2 benzene/di-*tert*-butyl peroxide.[20] It

Scheme 2. Photolysis Product Yields

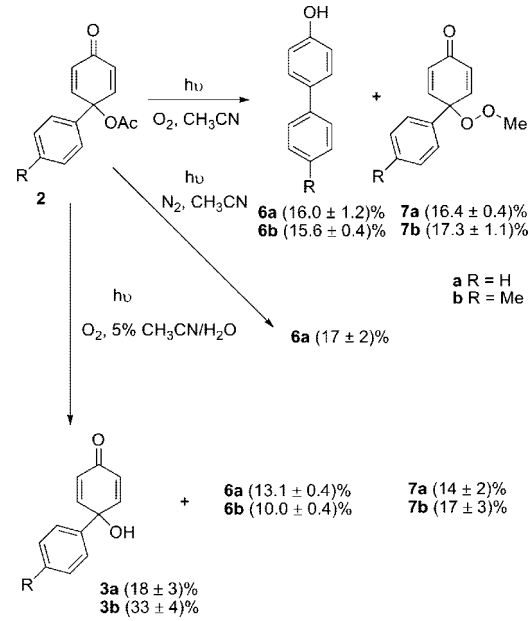

is concluded that the transient spectra in Figure 6 are due to **5a** and that the similar transient absorbance observed in Figure 1 is due to **5b**. The kinetics of decay of **5a** was examined in less detail than that of **5b**, but the transient absorbance at 340 nm in O_2-saturated CH_3CN decays in a biphasic manner very similar to that observed for **5b**. Rate constants are shown in Table 1.

Photolysis Products. Reaction products from steady-state photolysis of **2a** and **2b** are summarized in Scheme 2. The quinols (**3**) and the phenols (**6**) are known compounds.[14,16] The new peroxy compounds (**7**) were fully characterized. All compounds were isolated for identification, but yields are based on HPLC response factors. All reactions except the aqueous solution photolysis of **2b** were performed with an initial ester concentration of 2.5 mM. The aqueous solution photolysis of **2b** was performed with an initial ester concentration of 1×10^{-4} M.[17] Both **3** and **7** are significantly photoreactive under our conditions. To minimize this effect, product yields for the reactions run at 2.5 mM were obtained at early reaction times corresponding to ca. 15−30% photoreaction. The aqueous solution photolysis of **2b** at lower concentration led to ca. 95% conversion after 45 s of irradiation. In this case the observed yields of **3b** and **7b** were corrected for the observed photolytic decomposition of the authentic materials under the reaction conditions.[17] Other minor products were detected by HPLC of photolysis mixtures. Most were not characterized, but one minor product of **2a** with a long HPLC retention time has an *m/e* of 337 by negative ion mass spectrometry. This mass corresponds to $(M - 1)^-$ for a dimer of **5a**. Since this material can be detected by negative ion mass spectrometry, it is likely to be a phenol, but it was not isolated since it is ≪1% of the photolysis product mixture of **2a** in CH_3CN. The peroxy product **7a** is not produced in N_2-saturated CH_3CN, and experiments in CD_3CN demonstrate that the methyl group in **7a** is derived from the acyl methyl of **2a**, not from the solvent. The quinol product **3a** or **3b** can be detected from the steady-state photolysis of **2a** or **2b** in aqueous solution, but these products cannot be detected during photolysis in CH_3CN. The quinols are also generated as the exclusive hydrolysis products of **2a** and **2b** in the absence of other nucleophiles.[14,16] The yields of **3a** and **3b** shown in Scheme 2 were either obtained under conditions in which the

Scheme 3. Possible Mechanism for the Formation of **7**

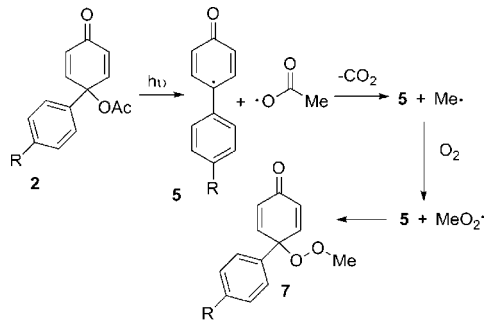

hydrolysis is too slow to compete with the photolysis reaction (**3a**) or corrected for the background hydrolysis reaction (**3b**).[17] Both **6** and **7** are detected during photolysis of **2a** and **2b** in O_2-saturated aqueous solution. This is consistent with observation of **5a** and **5b** during LFP of **2a** and **2b** in water.

The quinols **3a** and **3b** have been shown by solvent ^{18}O-labeling studies and N_3^--trapping experiments to be the products of the attack of H_2O on the oxenium ions **1a** and **1b** that are generated during hydrolysis of **2a** and **2b**.[14,16] The lack of generation of **3b** in CH_3CN is consistent with the LFP observations that show **1b** is not detected in CH_3CN, although it is generated in aqueous solution. Although **1a** was not directly detected by LFP, the generation of **3a** in the aqueous solution photolysis experiments indicates that this short-lived intermediate is generated by photolysis. The greater yield of **3b** compared to **3a** in the aqueous photolysis experiments may be due to transition state stabilization for photolytic generation of the more stable cation. The products **6** and **7** have not been detected during hydrolysis of **2a** or **2b** and are clearly generated from the intermediates produced by photolysis in CH_3CN. The phenols **6** are the expected products of hydrogen abstraction of **5**. A mechanism for generation of the peroxy compounds **7** that is consistent with the available data is shown in Scheme 3. Simple alkyl radicals, including a methyl radical, react with O_2 to form alkyl peroxyl radicals with rate constants of ca. 10^9 M^{-1} s^{-1}, while aryloxy radicals are unreactive with O_2.[32,33] Primary alkyl peroxyl radicals are relatively unreactive to hydrogen abstraction, double bond addition, and electron transfer.[32] Self-reaction occurs near the diffusion limit, but at low peroxyl radical concentration trapping by other radicals, such as **5**, should be competitive.[32]

Kinetic Modeling of the Decay of the Aryloxy Radicals. The biphasic decay kinetics observed for **5a** and **5b** can be fit by a double exponential rate equation, but this fit does not provide a mechanistic understanding of the decay processes for these radicals. It is known that aryloxy radicals are relatively long-lived species in solution that decay primarily by dimerization in the absence of radical traps.[21−27] In many cases in which there is a 4-alkyl or 4-aryl substituent, including **5a**, the dimerization is reversible and biphasic decay kinetics can be observed.[21,24,26] A mechanism similar to that shown in Scheme

Scheme 4. Kinetic for the Decay of **5**

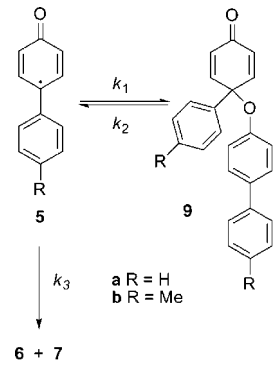

4 has been used to analyze these cases.[21,26] The dimer **9** was not isolated, but its structure is assumed to be analogous to the isolatable but highly reactive dimer obtained from DDQ oxidation of 2,6-di-*tert*-butyl-4-methylphenol.[28] This scheme was applied to the decay of the absorbance of **5b** at 360 nm in O_2-saturated 5% CH_3CN/H_2O or at 350 nm in both O_2- and Ar-saturated CH_3CN and to the decay of the absorbance of **5a** at 340 nm in O_2-saturated CH_3CN. The scheme was utilized because of the biphasic nature of the decay of the absorbance under these conditions and because the negligible yields of dimeric products observed in these photolyses suggest that **9** does not have an efficient pathway to lead directly to stable dimeric products. The monomeric products **6** and **7** are clearly obtained from **5** in processes that are not kinetically first-order, but a pseudo-first-order rate constant, k_3, can be used to describe these processes under reaction conditions in which species other than **5** are held at constant concentration. Since the initial concentrations of **5a** and **5b** in the LFP experiments are $\leq 3 \times 10^{-5}$ M (see below) this may be the case.

Absorbance vs time data were fit to the mechanism of Scheme 4 using a Powell fitting algorithm implemented in the KINTECUS kinetics simulation program.[34] The three rate constants k_1/ϵ, k_2, k_3 and the initial ($t = 0$) absorbance were used as variable parameters to optimize the fit. Examples of fits are shown in Figure 7, and fitted rate constants are gathered in Table 3.

Evaluation of the rate constant k_1 requires knowledge of the extinction coefficient, ϵ, for **5a** or **5b** at its short wavelength λ_{max} in the 340−360 nm range. The previously measured extinction coefficient for **5a** at the long wavelength absorbance band (502 nm) in 1:2 benzene/di-*tert*-butyl peroxide of 2580 M^{-1} cm^{-1} provides an estimate of ϵ at 340 nm for **5a** of 1.9×10^4 $M^{-1}cm^{-1}$ based on the observed absorbance ratio at λ_{max} of the two bands for **5a** in CH_3CN.[20] The same extinction coefficient was assumed for **5b** at its short wavelength λ_{max} in both CH_3CN and the aqueous solution. The error limit for ϵ may exceed ±50%, but it provides a reasonable estimate of the initial concentration of **5a** or **5b** of ca. $(1-3) \times 10^{-5}$ M in all the LFP experiments. This is 3%−10% of the initial concentrations of **2a** or **2b** present in solution. Estimates for k_1 are provided in Table 3. The values are 5−10-fold less than the expected diffusion limit. Previously measured dimerization rate constants of aryloxy radicals near room temperature have varied from ca. 10^7 M^{-1} s^{-1} to the approximate diffusion controlled limit of $(5-6) \times 10^9$ M^{-1} s^{-1} in solvents as diverse as benzene,

(32) (a) Neta, P.; Huie, R. E.; Ross, A. B. *J. Phys. Chem. Ref. Data* **1990**, *19*, 413–513. (b) Marchaj, A.; Kelley, D. G.; Bakac, A.; Espenson, J. H. *J. Phys. Chem.* **1991**, *95*, 4440–4441.

(33) (a) von Sontag, C.; Schuchmann, H.-P. *Angew. Chem., Int. Ed. Engl.* **1991**, *30*, 1229–1253. (b) Hunter, E. P. L.; Desrosiers, M. F.; Simic, M. G. *Free Radical Biol. Med.* **1989**, *6*, 581–585. (c) Berho, F.; Lesclaux, R. *Chem. Phys. Lett.* **1997**, *279*, 289–296. (d) Platz, J.; Nielson, O. J.; Wallington, T. J.; Ball, J. C.; Hurley, M. D.; Straccia, A. M.; Schneider, W. F.; Sehested, J. *J. Phys. Chem. A* **1998**, *102*, 7964–7974.

(34) Ianni, J. C. *Kintecus*, Windows Version 3.95, 2008, http://www.kintecus.comm/.

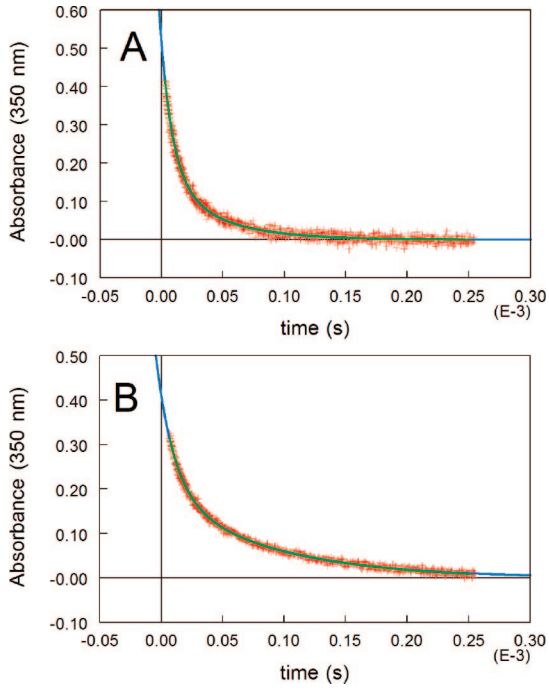

Figure 7. Kinetic fits for absorbance of **5b** at 350 nm vs time in (A) O_2-saturated CH_3CN and (B) Ar-saturated CH_3CN. Blue lines: the fit to a biphasic first-order rate equation (Table 1). Green lines: the fit to the kinetic mechanism of Scheme 4 (Table 3). ~90% of the data points were removed for clarity, but all data points were used for the fits.

CCl_4, and water.[21−25,27] The dimerization rate constant of **5a** in benzene at 30 °C is reported to be 3.4×10^7 M^{-1} s^{-1}.[23] Dimerization rate constants for several other aryloxy radicals in benzene are about an order of magnitude smaller than those for the same radicals in water, so our values for k_1 appear to be in reasonable agreement with the limited available data.[23]

The difference between k_1 values in aqueous solution and in CH_3CN for **5b** should not be over interpreted considering our assumptions concerning the magnitude of ϵ. Comparisons of the rate constants for **5b** in O_2-saturated CH_3CN with those in Ar-saturated CH_3CN show that the most significant difference is in k_3. The two rate constants that describe the dimerization equilibrium (k_1 and k_2) are quite similar under the two reaction conditions, and the dimerization equilibrium constant, $K_d = k_1/k_2$, is invariant at 3.1×10^4 M^{-1} under both reaction conditions, but k_3 in O_2-saturated CH_3CN is 2.4-fold larger than that in Ar-saturated CH_3CN. The relatively small effect of O_2 on the decay kinetics of **5b** is consistent with the reported lack of reactivity of aryloxy radicals with O_2.[33] The observed increase in k_3 in O_2-saturated CH_3CN is consistent with the proposed role of O_2 in the formation of **7b** (Scheme 3). The dimerization equilibrium for **5a** in O_2-saturated CH_3CN appears to be very similar to that of **5b** with a K_d of 2.4×10^4 M^{-1}, but k_3 is somewhat smaller for **5a** in O_2-saturated CH_3CN than k_3 for **5b** under the same reaction conditions. We do not understand the reasons for the substituent effect on k_3. Speculation on the nature of the effect would not be warranted at this time, since the decay processes represented by k_3 are quite complicated and we have not identified all of the products generated from the decay of **5a** and **5b**. The dimerization equilibrium constants measured here for **5a** and **5b** appear to be in the range of K_d measured for other aryloxy radicals.[21,26,27] For example, K_d for 2,6-di-*tert*-butyl-4-methylphenoxyl has been measured at room temperature as 6×10^4 M^{-1} in benzene and 1×10^6 M^{-1} in CCl_4.[21,26] For a more closely related radical, 2,4-dicyclohexyl-4-phenylphenoxyl, K_d is 2.5×10^4 M^{-1} at 20 °C in propanol.[27]

Conclusions

While hydrolysis of the quinol esters **2** with electron-donating substituents on the distal ring generates the aryloxenium ions **1** exclusively based on the quantitative yield of the quinols **3** and results of N_3^--trapping, common ion effects, and ^{18}O-labeling studies,[14−16] photolysis of these esters in aqueous solution generates both **1** and aryloxy radicals **5**. Product yields from photolysis of **2a** and **2b** suggest that photolytic generation of **1** is more favorable for the ester with the more electron-donating substituent, **2b**. Only **1b** was detected directly after nanosecond LFP at 266 nm because the lifetime of **1a** is too short for detection. The ion **1b** with λ_{max} 460 nm was characterized by the N_3^--dependence of its decomposition kinetics, by comparison of k_{az}/k_s measured directly with the same ratio measured by N_3^--trapping of the hydrolysis reaction, and by the comparison of the TR^3 spectrum of the intermediate with calculated vibrational transitions at the B3LYP/6-31G(d) level of theory. The agreement between calculated and observed transitions indicates that the calculated structure is an accurate representation of the cation. That structure indicates that **1b** should largely be considered as a 4-(*para*-tolyl)-1-oxo-2,5-cyclohexadienylcarbenium ion (resonance structure II of Figure 4) with significant charge delocalization into the substituent ring. The strong dependence of cation lifetimes on the substituent in the distal ring and the nature of the hydrolysis reaction products, **3**, are consistent with this interpretation.

The excellent agreement of the direct measurement of the lifetime of **1b** with the indirect measurements made by N_3^--trapping of the hydrolysis reaction of **2b** provides confidence in the indirect lifetime estimates we have made for several other 4′-substituted biphenylyloxenium ions (MeO, H, Br).[16,17] Ren and McClelland have measured the lifetimes of the corresponding nitrenium ions under similar conditions (20 vol% CH_3CN/H_2O, 20 °C).[35] A plot of log k_s for the biphenylyloxenium ions vs log k_s for the corresponding biphenylylnitrenium ions (Figure 8) shows that relative substituent effects on the stabilities of these ions are nearly identical (slope $\approx$ 1.0), although the nitrenium ions are ca. 30-fold more stable than the corresponding oxenium ions within the 3 orders of magnitude range of cation stabilities that can be compared. This is surprising given the results of the DFT calculations that show somewhat more charge delocalization into the distal rings of the biphenylyloxenium ions. This suggests that the oxenium ions would be more sensitive to substituent effects in the distal ring, which would be manifested by a slope > 1.0. The calculated differences are not large though, and compensating factors such as differential solvation of the more polar oxenium ions could mask the expected effect.

Although **1b** is only generated during photolysis of **2b** in water, the aryloxy radical **5b** can be detected after LFP in both aqueous solution and CH_3CN. The unsubstituted radical **5a** can also be detected after LFP of **1a** in both solvents. The radicals appear to be the exclusive initial photolysis products in CH_3CN, based on UV−vis spectra taken after LFP and on isolated product yields. These radicals were characterized by their reaction products, by comparison with the published UV−vis spectrum of **5a**, and by modeling of their decay kinetics.

(35) Ren, D.; McClelland, R. A. *Can. J. Chem.* **1998**, *76*, 78–84.

Table 3. Rate Constants Derived from Kinetic Modeling to Scheme 4

intermediate, reaction conditions[a]	k_1/ϵ (cm s^{-1})	k_1 (M^{-1} s^{-1})	k_2 (s^{-1})	k_3 (s^{-1})
5b, 5% CH_3CN/H_2O, O_2 sat	$(9.9 \pm 0.5) \times 10^4$	$(1.9 \pm 0.9) \times 10^9$	$(1.7 \pm 0.1) \times 10^4$	$(2.8 \pm 0.2) \times 10^4$
5b, CH_3CN, O_2 sat	$(4.1 \pm 0.2) \times 10^4$	$(7.8 \pm 3.9) \times 10^8$	$(2.5 \pm 0.1) \times 10^4$	$(5.2 \pm 0.2) \times 10^4$
5b, CH_3CN, Ar sat	$(3.0 \pm 0.1) \times 10^4$	$(5.7 \pm 2.9) \times 10^8$	$(1.8 \pm 0.2) \times 10^4$	$(2.2 \pm 0.1) \times 10^4$
5a, CH_3CN, O_2 sat	$(2.4 \pm 0.2) \times 10^4$	$(4.6 \pm 2.3) \times 10^8$	$(1.9 \pm 0.3) \times 10^4$	$(1.1 \pm 0.3) \times 10^4$

[a] Reaction conditions are the same as those described in Table 1. Average rate constants were obtained from fits of three to five independent runs under each set of reaction conditions. The error limits for k_1/ϵ, k_2, and k_3 are the standard deviations of the average values. The error limit for k_1 also includes an estimate of the error limit in the value of ϵ.

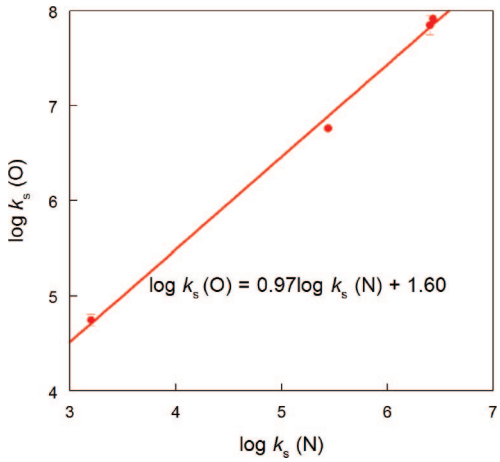

Figure 8. Plot of log k_s for substituted biphenylyl oxenium ions (O) vs log k_s for the corresponding nitrenium ions (N).

Although the esters **2** with electron-donating substituents on the distal ring generate trappable oxenium ions during hydrolysis, those with electron-withdrawing substituents (R = CN, NO_2) do not.[16] Instead, these esters react directly with nucleophiles such as N_3^- via kinetically bimolecular processes that appear to be S_N2' in nature.[16] The photochemistry of these electron-poor esters has not been reported. Although they are unlikely to lead to detectable singlet oxenium ions, they could be sources of triplet oxenium ions and/or aryloxy radicals.[18] We have begun to explore the photochemistry of these esters with an emphasis on their triplet sensitized photochemistry.

Experimental Section

Laser Flash Photolysis and Kinetics. Laser flash photolysis (LFP) was carried out using a Nd:YAG laser (266 nm, ca. 5 ns pulse) with a 1 cm light path. All reactions were performed at ambient temperature (22 °C). Solutions of **2a** and **2b** were prepared in O_2 or Ar saturated pH 7.1, 0.02 M phosphate buffer (5 vol% CH_3CN-H_2O, $\mu = 0.5(NaClO_4)$) or in O_2 or Ar saturated CH_3CN by injecting 15 μL of a ca. 0.04 M stock solution of **2a** or **2b** into 3 mL of solution, so that the initial concentrations were ca. 2.5×10^{-4} M. These solutions had an absorbance of ca. 0.50 to 0.75 at 266 nm with a 1 cm light path. Since both **2a** and **2b** undergo slow hydrolysis under these conditions, all solutions were used promptly after mixing, and experiments were completed within 5 min after mixing. Concentrations of N_3^- were in the range from 0 to 6 mM.

Transient absorbance spectra were monitored in the range 280−540 nm. Initial spectra were obtained with a delay of 20 ns after the laser pulse. Subsequent spectra were obtained at times dictated by the quenching of transient bands generated by LFP of **2b** at 360 and 460 nm in aqueous solution and at 350 and 575 nm in CH_3CN, and for **2a** at 350 nm in aqueous solution and 340 nm in CH_3CN. All transient spectra were collected over a 20 ns time window. Kinetics measurements for **2b** were made at 360 and 460 nm in aqueous solutions and at 350 and 575 nm in CH_3CN, for time spans that ranged from 1.25 to 250 μs depending on quenching rates of individual intermediates. Kinetics measurements for **2a** were made at 340 nm in CH_3CN. Kinetics measurements at all wavelengths were averaged three to five times. Between each measurement, the sample was remixed to avoid depletion of reactants within the volume of the cuvette exposed to the flash. Kinetics traces were fit to either a standard first-order rate equation containing a single exponential (460 nm) or a rate equation containing a double exponential (340, 350, 360, 575 nm). All data at $t \geq 10$ ns were used for the first-order fits at 460 nm; delays of 1 to 7 μs were used for the data taken at the other wavelengths. The delays were necessitated by fast decaying transients that disappeared at early reaction times.

Fitting of the absorbance vs time data taken at 360 nm in aqueous solution and at 340 and 350 nm in CH_3CN to the mechanism of Scheme 4 was performed with the Kintecus software package.[34] A small background absorbance that remained after decay of the transient of ca. 0.005−0.02 AU (<5% of the initial absorbance) was subtracted from the data before curve fitting. The four parameters k_1/ϵ, k_2, k_3, and the initial absorbance were used as adjustable parameters to optimize the fit. Approximately 1.2×10^4 data points were used in each individual fit. The Powell fitting algorithm was employed. Adjusted r^2 values for individual fits were in the range 0.85−0.91 with estimated standard deviations of the model of 0.005−0.015 AU. Pearson's r coefficient for each individual fit was in the range 0.90−0.96, and the Shapiro−Wilk W-test for Gaussian normality gave $W = 0.96-0.98$ with $P = 0.14-0.33$. Standard deviations of the individual fitting parameters were estimated from averages of 3 to 5 independent kinetic runs under each reaction condition.

Steady State Photolysis Experiments. The detailed procedures for steady state photolysis in aqueous solutions in a Rayonet photochemical reactor in a jacketed quartz vessel kept at 15 °C have been published.[17] The following modifications were made for photolysis in CH_3CN. UVC lamps that have emission (ca. 90% of total lamp energy) in the range 235−280 nm with a sharp maximum at 254 nm were used as the UV source. The desired amount of **2a** or **2b** was dissolved in ca. 1 mL of CH_3CN. This solution was transferred into 100 mL of O_2 or N_2 saturated CH_3CN in the photolysis reactor by disposable pipet. Reaction solutions were generated with initial concentrations of 2.5×10^{-3} M. Slow O_2 or N_2 bubbling was continued throughout the photolysis. The photolysis was initiated after the addition of **2a** or **2b** was complete, and the reaction solution was fully mixed. Irradiation times were variable, ranging from 3 to 15 min. The progress of photolysis as a function of irradiation time was monitored by HPLC. The HPLC conditions for monitoring the photolysis of **2b** have been published.[17] The HPLC conditions for **2a** were slightly modified (C-8 reversed phase column, 60/40 MeOH/H_2O eluent, 1 mL/min, monitored by UV absorbance at 221 and 238 nm).

Product Studies. The quinols **3a** and **3b** and the phenols **6a** and **6b** were identified by direct comparison to authentic samples.[14,16] Quantification of all products was obtained by calibration of HPLC peak areas with those of known concentrations of the photolysis products. A general procedure for isolation of photolysis products **7a** and **7b** is as follows. When the yield of these products reached a maximum, based on HPLC analysis (typically after 9−12 min of irradiation at initial concentrations of **1a** or **1b** of 2.5×10^{-3} M),

CH_3CN was removed from the reaction mixture by room temperature rotary evaporation under vacuum. An initial separation of photoproducts was performed by radial chromatography on silica gel using 60/40 hexanes/EtOAc. The fraction containing **7** was evaporated to dryness under vacuum, and the residue was redissolved in 10 mL of CH_2Cl_2 and washed with cold 1 M aqueous NaOH (2 × 5 mL) and cold saturated aqueous $NaHCO_3$ (2 × 5 mL). The CH_2Cl_2 solution was dried over Na_2SO_4 before the solvent was evaporated. The final purification of **7** was carried out by radial chromatography on silica gel with a different solvent system: 97.5/2.5 CH_2Cl_2/CH_3CN. Purified products were subjected to HPLC analysis before final characterization.

4-(Methylperoxy)-4-phenylcyclohexa-2,5-dienone (7a). Clear oil at room temperature. IR (thin film) 3060 (w), 2965 (w), 1668, 1630, 1449, 1390, 1165, 1063, 1000, 855, 752, 696 cm^{-1}; ^1H NMR (500 MHz, CD_2Cl_2) δ 3.91 (3H, s), 6.31(2H, d, J = 10.5 Hz), 7.03 (2H, d, J = 10 Hz), 7.38 (5H, m); ^{13}C NMR (125.8 MHz, CD_2Cl_2) δ 64.44, 81.35, 126.27, 129.26, 129.33, 129.73, 137.13, 148.50, 185.60; LC/MS (ESI, positive) *m/e* 192 $(M + Na - CH_3O_2)^+$, 217 $(M + H)^+$, 239 $(M + Na)^+$; High-resolution MS (ES, positive), $C_{13}H_{12}O_3Na$ (M + Na) requires 239.0684, found 239.0694.

4-(Methylperoxy)-4-(4′-methylphenyl)cyclohexa-2,5-dienone (7b). Clear oil at room temperature. IR (thin film) 3030 (w), 2963 (w), 1668, 1630, 1390, 1165, 1065, 1005, 958, 856, 815 cm^{-1}; ^1H NMR (500 MHz, CD2Cl2) δ 2.34 (3H, s), 3.90 (3H, s), 6.30 (2H, d, J = 10 Hz), 7.03 (2H, d, J = 10.5 Hz), 7.18 (2H, d, J = 8.0 Hz), 7.29 (2H, d, J = 8.5 Hz); ^{13}C NMR (125.8 MHz, CD_2Cl_2) δ 21.19, 64.41, 81.25, 126.18, 129.57, 129.90, 134.02, 139.56, 148.73, 185.63; LC/MS (ESI, positive) *m/e* 206 $(M + Na - CH_3O_2)^+$, 253 $(M + Na)^+$, 269 $(M + K)^+$; High-resolution MS (ES, positive), $C_{14}H_{14}O_3Na$ (M + Na) requires 253.0841, found 253.0817.

Nanosecond Time-Resolved Resonance Raman (ns-TR^3) Experiments. Stock solutions of 10 mM **2b** were prepared in CH_3CN and kept cool in an ice−water bath. 0.015 M Na_2HPO_4/0.005 M NaH_2PO_4 buffered distilled water and pure CH_3CN were also kept in the ice−water mixture. In each run of the experiment, 4 mL of **2b** stock solution were mixed with 16 mL of buffered water or CH_3CN to make a fresh 20 mL sample solution, which was immediately subjected to the TR^3 experiment. The experiment was accomplished within 2 min after the solution had been made to avoid any noticeable sample decomposition or photoproduct accumulation.

A brief description of the apparatus for the ns-TR^3 experiment is given here. A more detailed description is published elsewhere.[36,37] Two Nd:YAG nanosecond pulsed lasers in conjunction with hydrogen Raman shifters were used to produce the different laser wavelengths employed in the ns-TR^3 experiments. The fourth harmonic of a Nd:YAG laser (266 nm) was employed as the pump pulse. The third harmonic of a Nd:YAG laser (354.7 nm) and the first anti-Stokes Raman shifted line of the 532 nm second harmonic (435.7 nm) were employed as the probe laser pulses. Two Nd:YAG lasers here were electronically synchronized to each other by a pulse delay generator used to control the relative timing of two lasers. The relative timing of these two lasers was monitored using a fast photodiode and a 500 MHz oscilloscope. The jitter between the pump and probe laser pulses was observed to be less than 5 ns. The laser beams were lightly focused onto a flowing liquid stream of the sample using a near collinear backscattering geometry. The Raman scattered light was collected using a backscattering geometry and reflective optics that imaged the light through a depolarizer and the entrance slit of a 0.5 m spectrograph that dispersed the light onto a liquid nitrogen cooled CCD detector. The Raman signal was accumulated for 30 s before being read out to an interfaced PC computer, and ~10 to 20 of these Raman spectra were averaged to increase the signal-to-noise ratio of the spectrum obtained. The TR^3 spectra were determined by subtracting the pump−probe spectrum at negative 100 ns from the pump−probe spectra acquired at positive delay times so as to remove the solvent and precursor Raman bands. The known vibrational wavenumbers of the mixed solvent CH_3CN Raman bands were employed to calibrate the wavenumbers of the TR^3 spectra to an absolute accuracy of $\sim \pm 3$ cm^{-1} (and a relative accuracy of ± 1 to 2 cm^{-1} from scan to scan).

Density Functional Calculations. Density functional calculations on **1b** and **8b** were carried out using the Gaussian 03 suite of programs.[38] Geometry optimization of the ground-state oxenium ion was executed at the B3LYP/6-31G(d) level, and its verification as a minimum and derivation of IR and Raman vibrational frequencies and normal modes of vibration were executed using a harmonic frequency analysis, which afforded all real frequencies. Vibrational frequencies for comparison with experimental data were scaled by a factor of 0.9614 according to Scott and Radom.[39]

For comparative purposes, computed Raman intensities were weighted by a factor of 40 relative to the IR intensities to emulate relative experimental intensities of the most intense IR and Raman active bands in the resonance Raman spectrum. The combined, weighted theoretical spectrum was then scaled to approximate absolute resonance Raman intensities in the experimental spectrum which was first subjected to a biphasic baseline correction about the Rayleigh frequency.

Acknowledgment. We thank the Donors of the American Chemical Society Petroleum Research Fund (Grant No. 43176-AC4) for support of this work. Y.-T.W. thanks the Department of Chemistry and Biochemistry at Miami University for a Dissertation Fellowship, and K.J.J. thanks Miami University for an Undergraduate Summer Scholars award. The support of the NSF in Columbus and OSU Center for Chemical and Biophysical Dynamics is greatly appreciated. J.W. thanks the OSU Graduate School for a Presidential Fellowship. This work was supported in part by a grant from the Research Grants Council (RGC) of Hong Kong (HKU 7040/06P) to D.L.P. D.L.P. thanks the Croucher Foundation for the award of a Croucher Foundation Senior Research Fellowship (2006-07) and the University of Hong Kong for an Outstanding Researcher Award (2006).

Supporting Information Available: Table S1, containing all vibrational frequencies obtained during the TR^3 experiments; Figure S1, containing the vibrational modes calculated for **1b**; Figure S2, containing the 354.7 nm TR^3 spectra obtained after flash photolysis of **2b**; Figure S3, containing a comparison of the TR^3 spectra obtained using 354.7 and 435.7 nm probe lasers, in mixed aqueous solvent (20% CH_3CN 80% buffered water) and CH_3CN; Figure S4, containing the transient absorbance spectra recorded after 266 nm LFP of an Ar-saturated CH_3CN solution of **2b**; Tables S-2 and S-3, containing the Z-matrices for the optimized structures of **1b** and **8b** at the B3LYP/6-31G(d) level of theory; ^{13}C NMR spectra for **7a** and **7b**, an HMQC spectrum for **7a**, and complete ref 38. This material is available free of charge via the Internet at http://pubs.acs.org.

JA805336D

(36) (a) Li, Y.-L.; Leung, K. H.; Phillips, D. L. *J. Phys. Chem. A* **2001**, *105*, 10621–10625. (b) Li, Y. L.; Chen, D. M.; Phillips, D. L. *J. Org. Chem.* **2002**, *67*, 4228–4235.

(37) (a) Chan, P. Y.; Kwok, W. M.; Lam, S. K.; Chiu, P.; Phillips, D. L. *J. Am. Chem. Soc.* **2005**, *127*, 8246–8247. (b) Xue, J.; Guo, Z.; Chan, P. Y.; Chu, L. M.; But, T. Y. S.; Phillips, D. L. *J. Phys. Chem. A* **2007**, *111*, 1441–1451. (c) Xue, J.; Chan, P. Y.; Du, Y.; Guo, Z.; Chung, C. W. Y.; Toy, P. H.; Phillips, D. L. *J. Phys. Chem. B* **2007**, *111*, 12676–12684.

(38) Frisch, M. J. et al. *Gaussian 03*, revision E.01; Gaussian, Inc.: Wallingford, CT, 2005.

(39) Scott, A. P.; Radom, L. *J. Phys. Chem.* **1996**, *100*, 16502.